

Fluctuating Motor Forces Bend Growing Microtubules

NANDINI SHEKHAR,^{1,2} SRUJANA NEELAM,¹ JUN WU,^{1,3} ANTHONY J. C. LADD,¹ RICHARD B. DICKINSON,¹
and TANMAY P. LELE¹

¹Department of Chemical Engineering, University of Florida, Bldg 723, Gainesville, FL 32611, USA; ²Department of Biological Engineering, Massachusetts Institute of Technology, Cambridge, MA 02139, USA; and ³Department of Chemical and Biomolecular Engineering, University of Illinois, Urbana-Champaign, Urbana, IL 61801, USA

(Received 11 January 2013; accepted 10 May 2013)

Associate Editor Roger Kamm oversaw the review of this article.

Abstract—Despite their rigidity, microtubules in living cells bend significantly during polymerization resulting in greater curvature than can be explained by thermal forces alone. However, the source of the non-thermal forces that bend growing microtubules remains obscure. We analyzed the motion of microtubule tips in NIH-3T3 fibroblasts expressing EGFP-EB1, a fluorescent +TIP protein that specifically binds to the growing ends of microtubules. We found that dynein inhibition significantly reduced the deviation of the growing tip from its initial trajectory. Inhibiting myosin modestly reduced tip fluctuations, while simultaneous myosin and dynein inhibition caused no further decrease in fluctuations compared to dynein inhibition alone. Our results can be interpreted with a model in which dynein linkages play a key role in generating and transmitting fluctuating forces that bend growing microtubules.

Keywords—Microtubule bending, Dynein, Myosin.

INTRODUCTION

Microtubules play a central role in cell polarization,²⁸ migration,⁸ intracellular trafficking,⁶ cell division,²² and nuclear positioning.²⁶ *In vitro* experiments show that microtubules subjected to thermal forces have a persistence length on the order of millimeters,¹⁰ yet *in vivo* they exhibit bends on micron length scales. These bends develop primarily by deflections from linear tip trajectories rather than subsequent bending of intact microtubules,⁵ although initial bends may be amplified by compressive forces once the tip reaches the cell periphery⁴ or by the activity of cytoplasmic molecular motors.³²

Thermal forces are too small to explain the deflections of growing microtubules in living cells,⁵ and the causes of microtubule bending before the tips reach the cell periphery remains obscure. Growing microtubules can bend due to compressive stresses generated by polymerization against a barrier.^{2,4,7} Furthermore, the activity of myosin motors drives fluctuations in the cytomatrix, causing bending of existing microtubules *in vivo*³; myosin forces could bend growing microtubules by a similar mechanism. Processive microtubule motors such as dynein or kinesin can exert forces on the microtubule if they are anchored to the cytomatrix at the cargo-binding end.^{2,12,25,32} As the motor walks along the microtubule it pulls on the anchor point, resulting in a tensile force between the anchor and the point of attachment to the microtubule. Odde and coworkers² have suggested that the anterograde motion of buckling microtubules (moving towards the cell periphery) can be explained by microtubule-bound motor activity. In laser severing experiments with single microtubules in endothelial cells, newly created minus-ended microtubules bend (instead of straightening) in a dynein dependent manner,³² consistent with a model for dynein pulling forces along the entire length of the microtubule. This model also explains amplified buckles at the cell periphery and how the centrosome can be centered by an astral array of microtubules.³²

Given the athermal nature of forces that deflect growing microtubule tips,⁵ we reasoned that motor activity may also be responsible for bending growing microtubules. Using *in vivo* experiments, we show that bending of the trajectories of growing microtubule tips is significantly decreased in dynein-inhibited cells. Myosin-inhibition also decreases bends while kinesin-inhibition has no effect. Simultaneous inhibition of myosin and dynein in cells does not have any additional reduction in bending beyond that by inhibition

Address correspondence to Tanmay P. Lele, Department of Chemical Engineering, University of Florida, Bldg 723, Gainesville, FL 32611, USA. Electronic mail: tlele@che.ufl.edu
Srujana Neelam and Jun Wu contributed equally to this study.

81 of dynein alone. We interpret these results with a
82 mathematical model in which dynein linkages generate
83 and transmit fluctuating forces that bend growing
84 microtubules.

85 MATERIALS AND METHODS

86 *Cell Culture, Transfection, and Inhibition Experiments*

87 NIH-3T3 fibroblasts were cultured in Dulbecco's
88 Modified Eagle Medium (DMEM) (Mediatech,
89 Manassas, VA) with 10% Donor Bovine Serum (DBS)
90 (Gibco, Grand Island, NY). The cells were maintained
91 at 37 °C in humidified 5% CO₂. For microscopy the
92 cells were plated on 35 mm glass-bottomed dishes
93 (WPI, Sarasota, FL) and allowed to spread overnight
94 at 37 °C and 5% CO₂. The glass-bottomed dishes were
95 coated with 5 µg/mL fibronectin (BD Biocoat™,
96 Franklin Lakes, NJ) and kept at 4 °C overnight before
97 cell seeding.

98 In control experiments, cells were transiently
99 co-transfected with pGFP-EB1 (Addgene plasmid
100 17234) and DsRed and were incubated for 18–24 h prior
101 to plating. DsRed was expressed to allow comparisons
102 with cells expressing fluorescently labeled proteins such
103 as DsRed-CC1. In dynein inhibition experiments, cells
104 were co-transfected with DsRed-CC1 (Fig. S1) and with
105 mCherry-KHC in kinesin-1 inhibition experiments
106 (Fig. S1). DsRed-CC1 renders dynein inactive by com-
107 petitively binding to it and preventing dynein interac-
108 tions with dynactin^{31,32} while mCherry-KHC can
109 inhibit kinesin-1 by multiple mechanisms.²³ Transient
110 transfection of plasmids into cells was performed with
111 Lipofectamine™ 2000 transfection reagent (Life
112 Technologies, Invitrogen, Carlsbad, CA). Some cells
113 were treated for 30 min with 10 µM Y27632, which is a
114 Rho-kinase (ROCK) inhibitor that causes substantial
115 inhibition of non-muscle myosin.^{16,18}

116 *Confocal Microscopy*

117 The cells were imaged on a Leica SP5 DM6000
118 confocal microscope equipped with a 63X oil immer-
119 sion objective. During microscopy, cells were main-
120 tained at 37 °C in a temperature, CO₂, and humidity
121 controlled environmental chamber. In order to image
122 EGFP-EB1, a 488 nm laser with 10% power and an
123 appropriate GFP bandpass filter was used. Images
124 were taken at a resolution of 1024 × 1024 and with a
125 speed of 400 Hz, at a rate of 3 s/frame. The images
126 were further analyzed using LAS AF Lite (Leica Sys-
127 tems) software. For dynein and kinesin-1 inhibition
128 studies, expression of DsRed-CC1 and mCherry-KHC
129 was confirmed using epifluorescence microscopy.

Trajectory Analysis

130

131 Microtubule trajectories were constructed from an
132 analysis of EB1 movies using plusTipTracker, a
133 MATLAB based open source software package that
134 combines automated tracking, data analysis, and
135 visualization tools for analysis of movies of fluo-
136 rescently labeled microtubule plus end binding proteins
137 (+TIPs).¹ The software detects EB1 comets by appli-
138 cation of locally optimal thresholds using a watershed-
139 based technique. The track reconstruction is described
140 in more detail elsewhere.¹⁴

141 To test the accuracy of the software for our exper-
142 iments, we first measured the positional error in the
143 measurements. Fixed NIH-3T3 cells expressing EGFP-
144 EB1 were imaged for 2 min at three-second intervals.
145 Since the position of the tips is fixed, the variation in
146 the +TIP detection by the software provides an esti-
147 mate of the positional error. The deviation from the
148 mean was calculated for about eight tips. Figure S2
149 shows the plot of the frequency vs. the deviation from
150 the mean. Fitting a normal distribution to the data
151 yielded a standard deviation of 0.06 µm while the
152 average distance travelled by the tips in between suc-
153 cessive frames was 1.1 µm. Thus there is a 6% error in
154 the measurements, which was deemed to be small
155 enough to enable reliable tracking of the tips.

156 To reduce uncertainty due to positioning error in
157 the trajectory analysis, the initial direction of the tra-
158 jectory was determined by fitting a line to the first four
159 points in the trajectory. Each trajectory was first
160 translated to the origin and rotated onto the positive x -
161 axis by an angle that was determined by the slope of
162 the fitted line. The rotated trajectories thus had the
163 same initial direction. To quantitatively investigate
164 microtubule curvature, we next performed a Fourier
165 decomposition of the reconstructed trajectories,¹⁰ with
166 a trajectory length of 8 µm. The tangent angle,
167 $\theta = \tan^{-1}(dy/dx)$, was decomposed as a sum of sine
168 waves,

$$\theta(s) = \sqrt{\frac{2}{L}} \sum_{n=0}^{\infty} a_n \sin\left(\frac{n\pi s}{L}\right). \quad (1)$$

170 We assume that the microtubules are clamped at the
171 centrosome (i.e., a fixed orientation), so that the
172 boundary condition at the origin, $\theta(0) = 0$ is auto-
173 matically imposed by the basis functions.
174

175 From a set of N coordinates (x_k, y_k) making up a
176 trajectory, the length Δs_k and tangent angles θ_k of each
177 of the $(N - 1)$ segments that connect the coordinates
178 were calculated:

$$\Delta s_k = \left[(x_{k+1} - x_k)^2 + (y_{k+1} - y_k)^2 \right]^{\frac{1}{2}}, \quad (2)$$

180
$$\theta_k = \tan^{-1} \left[\frac{(y_{k+1} - y_k)}{(x_{k+1} - x_k)} \right]. \quad (3)$$

182 The amplitudes were determined by taking an
184 approximate Fourier transform of Eq. 1

$$a_n \cong \sqrt{\frac{2}{L}} \sum_{k=1}^N \theta_k \Delta s_k \sin\left(\frac{n\pi s_k^{\text{mid}}}{L}\right), \quad (4)$$

186 where

$$L = \sum_{k=1}^N \Delta s_k \quad (5)$$

188 and

$$s_k^{\text{mid}} = \Delta s_1 + \Delta s_2 + \dots + \Delta s_{k-1} + \frac{1}{2} s_k. \quad (6)$$

190

191 *Model for Dynein Force Generation*

192 Motor forces are included as linkages distributed
193 along the length of the microtubule, as illustrated in
194 Fig. 3a. We imagine that a particular segment of the
195 microtubule is occasionally captured by a cytoskeletal
196 bound dynein motor and bound for times of the order
197 of k_{off}^{-1} , where we take the dynein off rate to be of the
198 order of 1 s^{-1} .³² A segment of length h will capture a
199 dynein motor in a time step δt with a probability
200 $p = nhk_{\text{off}}\delta t$, where n is the (linear) density of dynein
201 motors per unit length of the microtubule, estimated at
202 about two cytoskeletal-bound motors per micron.³² On
203 average the binding and unbinding rates will balance at
204 the desired motor density n if each bound motor
205 unbinds with a probability $k_{\text{off}}\delta t$. Note that these for-
206 mulas assume that the binding and unbinding proba-
207 bilities are small, $k_{\text{off}}\delta t \ll 1$; more general formulas can
208 be derived in cases where $k_{\text{off}}\delta t$ is not small. The motor
209 model resembles that proposed by Nedelec and Foe-
210 thke²⁴; the main difference is that in our implementation
211 the motors only exist while bound to the microtubule
212 instead of being permanently bound to random positions
213 in the cytomatrix. It seems unlikely that this will cause
214 any substantial difference in the simulations.

215 A model for dynein force generation was con-
216 structed based on the following simplifying assump-
217 tions that are nevertheless consistent with what is
218 known about dynein-force generation: (1) The dynein-
219 cytoskeletal linkage is formed in a force-free state, with
220 a vector \mathbf{b}_i linking the point of attachment to the
221 microtubule, \mathbf{x}_i with the anchor point in the cytoma-
222 trix, \mathbf{a}_i . (2) The dynein motor walks towards the
223 microtubule minus end, with a force-dependent speed
224 δt until the tangential force reaches the stall force f_{max}
225 or the motor unbinds. The motor is displaced from its

initial position both by walking along the microtubule 226
and from the motion of the microtubule itself, 227

$$\mathbf{x}_i(t) = \mathbf{x}_i(0) - \int_0^t (v_{m,i} \mathbf{t} + \mathbf{v}) dt', \quad (7)$$

where \mathbf{v} is the velocity of the microtubule segment. The 229
motor walks with a speed $v_{m,i}$ in the direction of the 230
local tangent to the microtubule \mathbf{t} , which is formed by 231
assuming the filament is made up of straight segments 232
connecting the nodes. We assume a linear force 233
velocity relation varying from a maximum speed in 234
the force-free state, v_{max} to zero at the stall force, f_{max} 235
The coordinate s_i , which measures the position of the 236
motor along the contour length of the microtubule, is 237
incremented by $v_{m,i}\delta t$ at each time step, and the motor 238
position is then determined by interpolating from the 239
neighboring nodes. The velocity of the segment is 240
found by interpolating the nodal velocities. (3) The 241
initial distribution of directions of the microtubule- 242
cytomatrix linkage, \mathbf{b} , is isotropic with the anchor 243
points initialized as $\mathbf{a}_i(0) = \mathbf{x}_i(0) + \mathbf{b}_i$ To model the 244
action of the myosin network, the anchor points \mathbf{a}_i are 245
moved with random velocities, which represents the 246
motor-induced motions of the cytomatrix. Each an- 247
chor point is assumed to move with a constant velocity 248

$$\mathbf{a}_i(t) = \mathbf{a}_i(0) + \mathbf{v}_{a,i}t, \quad (8)$$

for as long as the motor remains bound. 250

Under these assumptions, both the displacement of 251
the motor from its binding and the motion of the an- 252
chor point can cause an extension of the dynein link- 253
age, $\mathbf{r}_i(t) = \mathbf{a}_i(t) - \mathbf{x}_i(t)$, with a linear force along the 254
linkage (Fig. 3a) 255

$$\mathbf{f}_i = \kappa \left(1 - \frac{b}{r_i} \right) \mathbf{r}_i. \quad (9)$$

It is possible for the motor to exert a compressive 258
force on the dynein-cytomatrix linkage if $\mathbf{b}\mathbf{t} < 0$ 259
However this is always transient since eventually the 260
motor will walk to a position such that $\mathbf{b}\mathbf{t} > 0$. 261

262 *Equation of Motion*

The strain energy in a bent elastic filament of length 263
 L (free from external couples) can be written as a line 264
integral of the mean-square curvature,¹⁷ 265

$$H = \frac{B}{2} \int_0^L C^2(s) ds, \quad (10)$$

where s is the distance along the filament arc, and B is 267
the bending modulus. If we discretize the filament 268
into N segments of uniform length $h = L/N$, then a 269

270 second-order approximation to the strain energy is
271 given by^{20,21}

$$H = \frac{Bh}{2} \sum_{n=1}^{N-1} C_n^2, \quad (11)$$

273 where the curvature C_n is related to the angle between
274 adjacent segments, $C_n^2 = 2(h^2 - \mathbf{r}_{n,n-1} \cdot \mathbf{r}_{n+1,n})/h^4$. The
275 discrete approximation to H can then be differentiated
276 to find the elastic force on each node of the filament. In
277 addition to the elastic forces, there is also a constraint
278 force that is required to maintain the length of the
279 individual segments, $\mathbf{r}_{n,n-1} \cdot \mathbf{r}_{n,n-1} = h^2$.^{20,21}

280 In the overdamped limit, the nodal velocities \mathbf{v}_n are
281 obtained from the force balance:

$$-\frac{\partial H}{\partial \mathbf{r}_n} + \mathbf{f}_n + \gamma \mathbf{v}_n h = 0, \quad (12)$$

283 where \mathbf{f}_n is the total force on node n from the motors
284 on neighboring segments. The friction coefficient γ is
285 taken to represent the background friction of the cel-
286 lular matrix; we take value of 10 Pa s, or 10 N m⁻² s,
287 based on measurements of microtubule relaxation in
288 dynein-inhibited cells.³²

289 RESULTS

290 *Fluctuations in Growing Microtubule Tips*

291 We tracked the position of EGFP-EB1 labeled
292 microtubule tips in cells using plusTipTracker and
293 microtubule trajectories were reconstructed from the
294 measured tip positions. The tips were tracked in a
295 region that encircled the centrosome, but not closer
296 than 5 μm to the cell periphery. This was done to
297 exclude events where the growing tip might experience
298 compressive loading as it grew against the membrane.
299 To avoid spurious tracks, each trajectory was visually
300 confirmed to be correctly detected and trajectories that
301 weren't reconstructions of the growth of a single tip
302 were discarded. A minimum of 12–13 cells were imaged
303 and 300–600 trajectories per condition were quantified.

304 Figure 1a shows the trajectory plots for growing
305 microtubules in normal cells. All trajectories were
306 translated to the origin and rotated so that the initial
307 direction was along the positive x -axis, as described in
308 “Materials and Methods” section. In control cells that
309 expressed DsRed the trajectories were observed to
310 spread out significantly over tens of seconds.

311 *Motor Activity Bends Growing Microtubules*

312 We next over-expressed DsRed-CC1 in NIH-3T3
313 fibroblasts to competitively inhibit dynein.^{31,32} The
314 spread in the trajectories was less in dynein-inhibited

cells compared to control cells (compare Figs. 1a and 315
1b). When kinesin was inhibited by expressing 316
mCherry-KHC,²³ the spread was similar to the control 317
cells (Fig. S3). 318

319 We next attempted to inhibit non-muscle myosin
320 activity with blebbistatin, a specific myosin II inhibi-
321 tor.¹⁵ However, at doses that inhibited myosin activity,
322 blebbistatin treatment caused a significant rounding of
323 cells making it difficult to track EB1 tips reliably in
324 these cells. We therefore treated cells with Y27632, a
325 ROCK inhibitor that has been shown to cause a large
326 decrease in non-muscle myosin activity without caus-
327 ing cell rounding.^{16,18} The spread of the trajectories on
328 Y27632 treatment is shown in Fig. 1c and appears to
329 be decreased when compared to control cells, but to a
330 lesser extent than in dynein-inhibited cells (Fig. 1b).

331 As all trajectories start at the origin and are initially
332 oriented along the positive x -axis, any deviation of the
333 trajectories in the y -direction is a measure of the
334 spread. One method of quantifying the effects of motor
335 inhibition on trajectory spread is to compare the var-
336 iance of the y positions of the tips at different times.
337 However, modest but statistically significant differ-
338 ences in tip speed were observed when dynein, kinesin,
339 or ROCK was inhibited (Fig. S4). Owing to the dif-
340 ferences in the polymerization velocity, we instead
341 chose to examine the length-dependence of the vari-
342 ance at each condition (Fig. 1d). The variance in dy-
343 nein-inhibited cells is decreased by a factor of two in
344 comparison with control cells. There is a smaller
345 decrease in variance in ROCK inhibited cells, but
346 there is no statistically significant difference between
347 kinesin-1 inhibited cells and control cells.

348 *Fourier Mode Analysis of Tip Trajectories*

349 To further characterize the deflections of polymer-
350 izing microtubules, we performed a Fourier mode
351 analysis (described in the “Materials and Methods”
352 section) on the measured trajectories. A comparison of
353 the Fourier mode amplitudes for different experimen-
354 tal conditions is shown in Fig. 2. Shape fluctuations in
355 control cells were significantly higher than those in
356 dynein-inhibited cells at almost all mode numbers
357 ($p < 0.05$ for mode 1 by Student's t test), indicating
358 that dynein linkages contribute significantly to the
359 bending of microtubule trajectories (Fig. 2a). In con-
360 trast, trajectories in cells where only kinesin was
361 inhibited showed no discernible differences from the
362 control cells (Fig. 2b). Inhibition of myosin only
363 reduced the mean-square amplitudes at some wave-
364 lengths, and to a lesser extent than inhibition of dynein
365 (Fig. 2c). Inhibition of both myosin and dynein
366 showed a similar reduction in mode amplitudes as
367 inhibition of dynein alone (Fig. 2d).

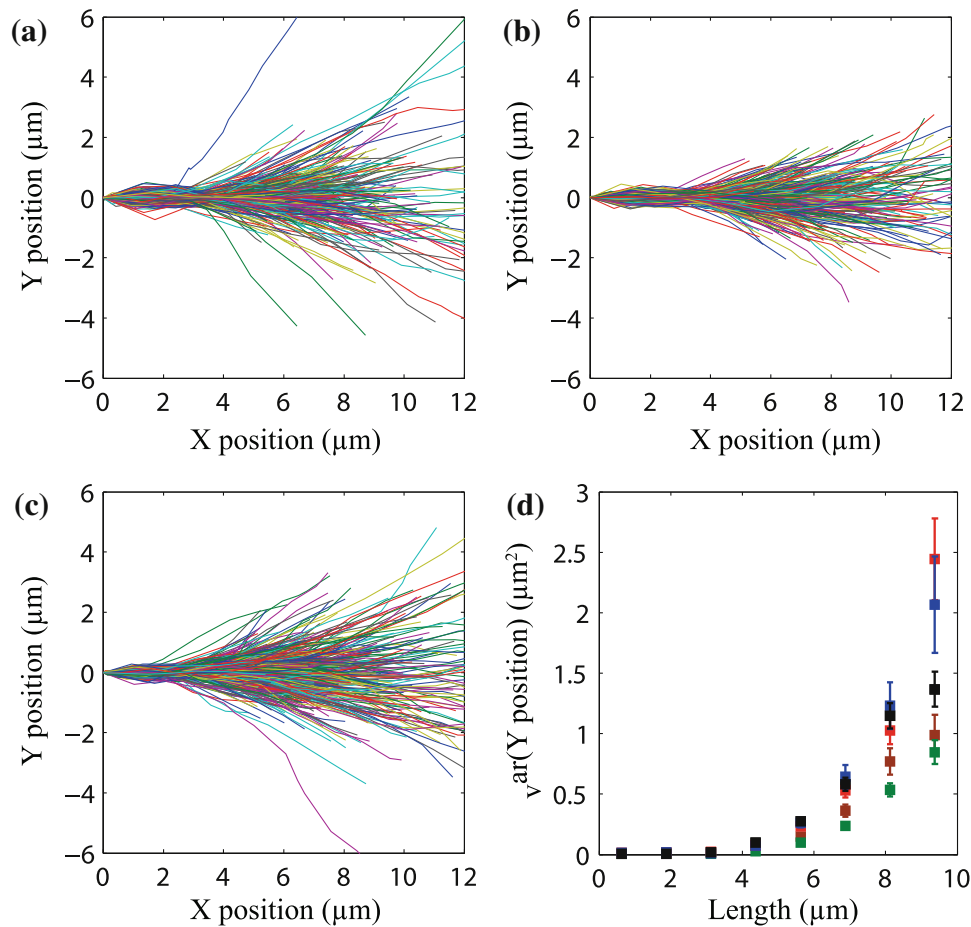


FIGURE 1. Motor activity causes bending during microtubule growth. Trajectories of growing microtubules under different conditions were reconstructed using plusTipTracker. Plots for growing microtubule trajectories are shown for (a) control cells, (b) dynein-inhibited cells, and (c) myosin-inhibited cells. In comparison to control cells, inhibition of dynein and myosin reduces the spread of the trajectories. Panel (d) shows a comparison of the length dependent variance under different conditions: control (red), kinesin inhibited (blue), myosin inhibited (black), DI (green), and dynein and myosin inhibited (brown). Errors bars indicate the standard error in the mean (SEM). About 12 cells and 300–600 trajectories were analyzed for each case.

368 These results suggest that both myosin and dynein
 369 contribute to bending the trajectories of microtubule
 370 tips. One possibility, consistent with these results, is
 371 that myosin motor-induced force fluctuations are
 372 transmitted primarily through dynein linkages between
 373 the microtubule and the actin cytoskeleton; blocking
 374 these linkages by CCI would then be sufficient to block
 375 both myosin-induced forces and dynein-induced forces
 376 on the polymerizing microtubules.

377 *Simulations of Fluctuations in Growing Microtubules*

378 In order to better understand the results of the
 379 motor-inhibition experiments, we used numerical sim-
 380 ulations of growing microtubules to investigate possi-
 381 ble mechanisms whereby microtubule trajectories are
 382 deflected by motor forces, either dynein or myosin
 383 generated. The cartoon in Fig. 3a illustrates the
 384 model for the motor forces. We assume that the

dynein–cytomatrix linkage is formed in a stress-free 385
 state; for simplicity we further assume that the 386
 microtubules grow in the basal plane of the cell and the 387
 linkage is also in the same plane, oriented randomly 388
 with respect to the tangent to the microtubule at the 389
 point of attachment. As the motor begins to walk 390
 along the microtubule it exerts a force along the line 391
 between the attachment point on the microtubule and 392
 the anchor point in the cytomatrix. This force has 393
 components parallel to and perpendicular to the local 394
 tangent direction that can deflect the microtubule as 395
 illustrated in Fig. 3a. The parameters for the micro- 396
 tubules and dynein motors (Table 1) are the same as in 397
 our previous simulations.³² 398

A typical simulation of a growing microtubule is 399
 illustrated in Movie 1 and Fig. 3b for the case where 400
 dynein is anchored to a stationary cytomatrix (i.e., 401
 $v_{a,i} = 0$). The dynein motors pull along the direction 402
 of the motor-anchor vector, indicated by the red lines, 403

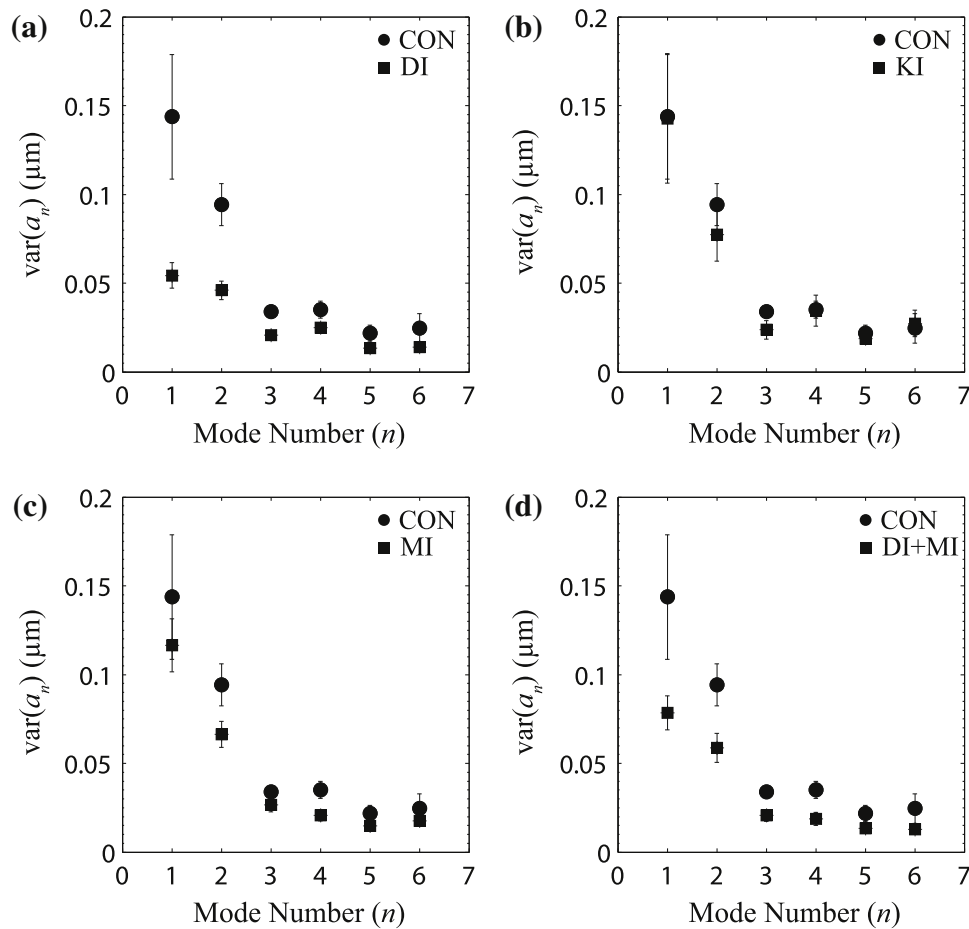


FIGURE 2. Fourier mode analysis of microtubule growth trajectories. The variance of Fourier amplitudes was calculated for each mode.¹⁰ Plots (a)–(d) show amplitude variances for different conditions (squares) in comparison to control cells (circles). Amplitude variances of microtubules in DI cells are less than half those of control cells (a), are unchanged in kinesin inhibited (KI) cells (b), and decreased in myosin inhibited (MI) cells (c). Simultaneous myosin and dynein inhibition (MI + DI) showed a similar reduction to dynein inhibition alone (d). The results suggest that dynein and myosin, but not kinesin contribute to microtubule bending. Error bars indicate SEM.

404 and so exert lateral as well as tangential forces. The
 405 microtubule can be significantly diverted from a
 406 straight-line path as shown in Fig. 3c, which shows the
 407 final configurations of 100 fully-grown ($8 \mu\text{m}$) micro-
 408 tubules. The variance of the tip position calculated
 409 from the simulated trajectories in Fig. 3c is about
 410 $0.8 \mu\text{m}^2$ at $8 \mu\text{m}$ length, which is somewhat less than
 411 that observed in experiments ($1.3 \mu\text{m}^2$ at $8 \mu\text{m}$,
 412 Fig. 1d). However in dynein-inhibited cells, there is
 413 still a significant variance in the tip position ($0.47 \mu\text{m}^2$
 414 at $8 \mu\text{m}$, Fig. 1d) which is much larger than can be
 415 accounted for by thermal forces alone. Since there are
 416 no such background fluctuations in the simulations
 417 and microtubules grow straight in the absence of
 418 motor forces, it is to be expected that the fluctuations
 419 in the tip positions are less than those observed in the
 420 experiments. The simulated variance in the tip posi-
 421 tions closely matches the observed *difference* between
 422 control cells and dynein-inhibited cells.

We next performed a Fourier decomposition on the
 simulated trajectories in Fig. 3c. The variance of the
 first bending mode, $\text{var}(a_1) = 0.09 \mu\text{m}$ is due entirely
 to dynein activity (no other effects are included in the
 simulation). This variance matches exactly to the
 reduction in variance of the first bending mode fol-
 lowing dynein inhibition, from $0.144 \mu\text{m}$ in control
 cells to $0.054 \mu\text{m}$ in dynein inhibited (DI) cells
 (Fig. 2a), i.e., $\text{var}(a_1^{\text{CON}}) - \text{var}(a_1^{\text{DI}}) = 0.09 \mu\text{m}$. How-
 ever, the observed effect of dynein on the second mode
 $\text{var}(a_2^{\text{CON}}) - \text{var}(a_2^{\text{DI}}) = 0.045 \mu\text{m}$ is not well repro-
 duced by the simulation result, $\text{var}(a_2) = 0.01 \mu\text{m}$.

Since myosin inhibition produced a measureable
 decrease in the variance of tip positions, we next
 investigated the influence of myosin forces on the
 microtubule tip trajectories. We used a simple model of
 myosin activity, where the anchor points of dynein on
 the cytomatrix move with a fixed velocity; here we
 choose $v_a = 0.05 \mu\text{m s}^{-1}$, which is consistent with

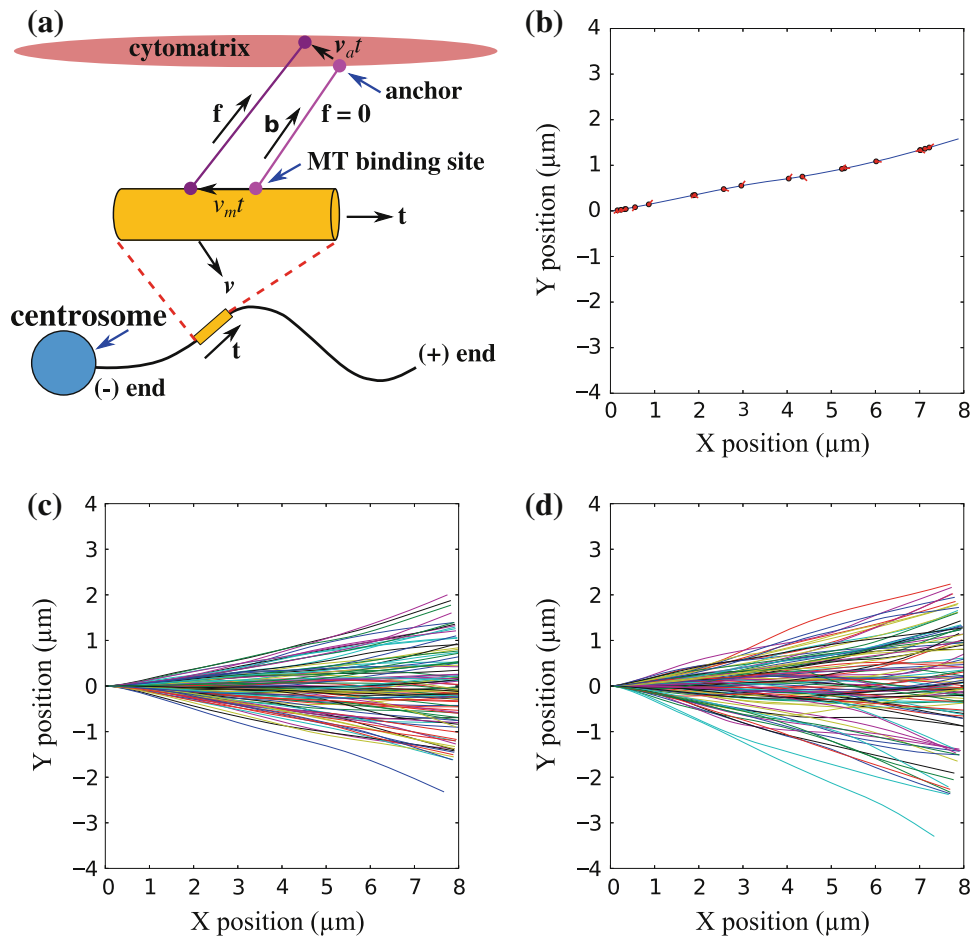


FIGURE 3. Numerical simulations of microtubule bending by dynein and myosin. The model for dynein and myosin force generation is illustrated in (a). A dynein–cytomatrix linkage is formed in a force-free state at time $t = 0$; the light mauve circles indicate the points of attachment to the microtubule and cytomatrix. As the motor walks along the microtubule, shown by the dark mauve circle, the linkage is extended and a force is exerted in the direction shown by the black arrow. In addition the anchor point in the cytomatrix may also be moved by myosin activity. The total force in the linkage is a combination of dynein and myosin activity. A simulation of filament growth is illustrated in (b), which shows the configuration of a microtubule polymerized to a contour length of $8 \mu\text{m}$. The red circles are the positions of the dynein motors and the red lines indicate the dynein–cytomatrix linkage. (c) and (d) show the trajectories of 100 different samples (in each case) under the action of dynein forces (stationary anchor points) and dynein plus myosin forces (moving anchors) respectively.

442 measurements of myosin motor speeds.³⁰ A simulation
 443 showing the growth of a typical microtubule with
 444 moving anchor points is shown in Movie 2. It can be seen
 445 that there is more curvature in the growing filament,
 446 which is reflected in larger values for the variance of the
 447 first bending mode $\text{var}(a_1)0.15 \mu\text{m}$. The larger deflec-
 448 tions and curvatures can also be seen in the trajectory
 449 plots of 100 sample microtubules (Fig. 3d). The ampli-
 450 tude of the second mode, $\text{var}(a_2) = 0.02 \mu\text{m}$, is larger
 451 than in the absence of cytoskeletal flow but still smaller
 452 than the experimental observations. Thus our models
 453 only account for the large scale fluctuations in micro-
 454 tubule shape, but not the detailed Fourier spectrum.

455 We found that the shapes of the microtubules were
 456 insensitive to variations in the dynein motor parameters.
 457 It is the mechanism of dynein pulling that tends to lead
 458 to deflected filaments rather than the exact motor

parameters. On the other hand the shapes are sensitive to 459
 the motion of the anchor points, which we used to rep- 460
 resent myosin-driven fluctuations in the cytomatrix The 461
 speed of the anchor points ($0.05 \mu\text{m s}^{-1}$) was less than 462
 typical myosin motor speeds ($0.15\text{--}0.2 \mu\text{m s}^{-1}$), based 463
 on the assumption that the cytomatrix moves more 464
 slowly than the motors pulling it. In future the compli- 465
 ance of the cytomatrix could be taken into account with 466
 a force balance on the myosin-actin network instead of a 467
 prescribed motion of the anchor points. 468

DISCUSSION 469

Despite their rigidity, microtubules in living cells 470
 contain both short-wavelength bends at the periphery 471
 and long-wavelength bends in the cell interior.^{2,5,10,32} 472

TABLE 1. Model parameters.

Symbol	Parameter	Range	Source	Value used
f_{\max}	Maximum dynein force	5–8 pN	9	8 pN
v_m	Dynein speed (no force)	$0.8 \mu\text{m s}^{-1}$	29	$0.8 \mu\text{m s}^{-1}$
κ	Dynein spring constant	$0.1\text{--}1 \text{ pN nm}^{-1}$	13,19	1 pN nm^{-1}
k_{off}	Dynein-nucleus off-rate	No value	32	1 s^{-1}
ρ	Dynein density	No value	32	$2 \mu\text{m}^{-1}$
N	Number of microtubules	200–500	11	100
v_{pol}	MT polymerization speed	$0.1\text{--}0.2 \mu\text{m s}^{-1}$	11,27	$0.1 \mu\text{m s}^{-1}$
ζ	Effective friction		32	10 Pa s
v_a	Myosin speed	$0.1\text{--}0.2 \mu\text{m s}^{-1}$	30	$0.1 \mu\text{m s}^{-1}$
B	Bending modulus	$24\text{--}30 \text{ pN nm}^{-2}$	13	25 pN nm^{-2}

473 The action of minus-end directed motors, specifically
 474 dynein, provides an explanation for both the short
 475 wavelengths and the localization of these buckles near
 476 the periphery.³² While growth of microtubules along
 477 curved paths has been proposed as the reason for long
 478 wavelength bends in the cell interior,⁵ the forces that
 479 cause growing microtubule tips to deflect from a
 480 straight path have remained unclear. In this paper, we
 481 suggest that forces bending the growing microtubule
 482 are transmitted to it by dynein. These forces may be
 483 generated by dynein activity itself, or by myosin forces
 484 that cause motion of dynein anchors in the cytomatrix.

485 Our results show that dynein and myosin inhibition
 486 significantly decrease the spread in microtubule tra-
 487 jectories, but kinesin inhibition does not have any
 488 noticeable effect. However, even when both dynein and
 489 myosin activity is suppressed, microtubules still spread
 490 considerably more than would be expected from ther-
 491 mal forces alone. Thus, there appears to be no single
 492 cause for the observed microtubule shapes; both dy-
 493 nein, myosin, and some, as yet undetected, causes
 494 (organelles or other motors) all contribute to the
 495 observed deflections.

496 The dynein–cytomatrix linkage plays both an active
 497 and a passive role in determining microtubule shapes.
 498 Dynein generates bends by its own motor activity
 499 (active) and it transmits myosin forces *via* the motion
 500 of the cytomatrix in the region of its anchor point
 501 (passive). In this view, inhibiting the dynein–cytoma-
 502 trix linkage by DsRed-CC1 prevents dynein from
 503 pulling on the microtubule but also inhibits transmis-
 504 sion of myosin forces to the microtubule. Assuming
 505 that the contributions of dynein and myosin are
 506 additive, a comparison of the variance of the first mode
 507 amplitudes suggests that about 40% of the stored
 508 bending energy comes from as yet unidentified sources,
 509 15% from myosin activity⁵ transmitted by stationary
 510 dynein linkages, and 45% from dynein motor activity
 511 as if pinned to a static cytomatrix.

An alternative explanation of the data is that myosin
 does not play a significant role in influencing filament
 shapes and that dynein accounts for about 60% of the
 filament bending energy. Myosin inhibition could re-
 duce the effectiveness of dynein molecules that are
 pulling on the microtubules because the F-actin network
 is less dense in the absence of myosin crosslinking.
 Inhibiting myosin in cells where dynein activity is also
 inhibited would then be expected to have no further ef-
 fect on the spread, while inhibiting myosin or dynein
 alone would decrease the deviation from straight paths.

Both these mechanisms are consistent with the
 experimental observations. To assess the plausibility
 of these different mechanisms, we carried out simu-
 lations of microtubule growth under the action of
 dynein and myosin motor forces. First, we investi-
 gated the possibility that cytoskeletal-bound dynein
 motors can produce bends in growing microtubules.
 We found that dynein motors produced significant
 deflections in the microtubule tips, as measured by
 the variance in the tip position for 100 microtubules
 (Fig. 3c). The variance in position for $8 \mu\text{m}$ segments,
 $\sim 0.8 \mu\text{m}^2$ correlates well with the difference in vari-
 ance in control cells ($\sim 1.2 \mu\text{m}^2$) and dynein-inhibited
 cells ($\sim 0.5 \mu\text{m}^2$). Moreover, simulations of the vari-
 ance in the amplitude of the first mode match the
 experimentally measured change in mode amplitudes
 when dynein is inhibited. We next implemented a very
 simple model where the anchor points of the dynein
 motors move with randomly chosen velocities, mim-
 icking the effect of myosin driven flow in the cyto-
 matrix. Larger bends were observed when the
 fluctuations in cytomatrix were included, but these
 are too large to be consistent with the difference
 between control cells and those with dynein–cytoma-
 trix linkages inhibited. Thus the simulations support
 the hypothesis that dynein is the key driver of fluc-
 tuations in microtubule shape, with myosin generated
 forces playing at most a secondary role.

552 **ELECTRONIC SUPPLEMENTARY MATERIAL**

553

554 The online version of this article (doi:10.1007/s)
555 contains supplementary material, which is available to
556 authorized users.

557 **ACKNOWLEDGMENTS**

558 The following grant supported this work: NSF CMMI
559 0954302, NSF CMMI 0927945, NIH GM102486, and
560 NSF CTS-0505929. DsRed-CC1 and mCherry-KHC
561 were gifts from Prof. Trina Schroer (Johns Hopkins
562 University) and Prof. Kristen Verhey (University of
563 Michigan). We thank the anonymous referee for pointing
564 out the appropriateness of sine functions in the curvature
565 analysis rather than a cosine basis.
566

567 **REFERENCES**

568 ¹Applegate, K. T., S. Besson, A. Matov, M. H. Bagonis, K.
569 Jaqaman, and G. Danuser. plusTipTracker: quantitative
570 image analysis software for the measurement of microtu-
571 bule dynamics. *J. Struct. Biol.* 176:168–184, 2011.
572 ²Bicek, A. D., E. Tuzel, A. Demtchouk, M. Uppalapati,
573 W. O. Hancock, D. M. Kroll, and D. J. Odde. Anterograde
574 microtubule transport drives microtubule bending in LLC-
575 PK1 epithelial cells. *Mol. Biol. Cell* 20:2943–2953, 2009.
576 ³Brangwynne, C. P., G. H. Koenderink, F. C. MacKintosh,
577 and D. A. Weitz. Nonequilibrium microtubule fluctuations
578 in a model cytoskeleton. *Phys. Rev. Lett.* 100:118104–
579 118104, 2008.
580 ⁴Brangwynne, C. P., F. C. MacKintosh, S. Kumar, N. A.
581 Geisse, J. Talbot, L. Mahadevan, K. K. Parker, D. E.
582 Ingber, and D. A. Weitz. Microtubules can bear enhanced
583 compressive loads in living cells because of lateral rein-
584 forcement. *J. Cell Biol.* 173:733–741, 2006.
585 ⁵Brangwynne, C. P., F. C. MacKintosh, and D. A. Weitz.
586 Force fluctuations and polymerization dynamics of intra-
587 cellular microtubules. *Proc. Natl. Acad. Sci. U.S.A.*
588 104:16128–16133, 2007.
589 ⁶Caviston, J. P., and E. L. Holzbaun. Microtubule motors at
590 the intersection of trafficking and transport. *Trends Cell*
591 *Biol.* 16:530–537, 2006.
592 ⁷Dogterom, M., and B. Yurke. Measurement of the force-
593 velocity relation for growing microtubules. *Science*
594 278:856–860, 1997.
595 ⁸Etienne-Manneville, S. Actin and microtubules in cell
596 motility: which one is in control? *Traffic* 5:470–477, 2004.
597 ⁹Gennerich, A., and S. L. Reck-Peterson. Probing the force
598 generation and stepping behavior of cytoplasmic dynein.
599 *Methods Mol. Biol.* 783:63–80, 2011.
600 ¹⁰Gittes, F., B. Mickey, J. Nettleton, and J. Howard. Flexural
601 rigidity of microtubules and actin filaments measured from
602 thermal fluctuations in shape. *J. Cell Biol.* 120:923–934, 1993.
603 ¹¹Glikzman, N. R., R. V. Skibbens, and E. D. Salmon.
604 How the transition frequencies of microtubule dynamic

instability (nucleation, catastrophe, and rescue) regulate
microtubule dynamics in interphase and mitosis: analysis
using a Monte Carlo computer simulation. *Mol. Biol. Cell*
4:1035–1050, 1993.
¹²Hamaguchi, M. S., and Y. Hiramoto. Analysis of the role
of astral rays in pronuclear migration in sand dollar eggs by
the Colcemid-UV method. *Dev. Growth Differ.* 28:143–156,
1986.
¹³Howard, J. *Mechanics of Motor Proteins and the Cyto-
skeleton.* Sunderland, MA: Sinauer, 2001.
¹⁴Jaqaman, K., D. Loeke, M. Mettlen, H. Kuwata, S.
Grinstein, S. L. Schmid, and G. Danuser. Robust single-
particle tracking in live-cell time-lapse sequences. *Nat.*
Methods 5:695–702, 2008.
¹⁵Kovacs, M., J. Toth, C. Hetenyi, A. Malnasi-Csizmadia,
and J. R. Sellers. Mechanism of blebbistatin inhibition of
myosin II. *J. Biol. Chem.* 279:35557–35563, 2004.
¹⁶Kumar, S., I. Z. Maxwell, A. Heisterkamp, T. R. Polte,
T. P. Lele, M. Salanga, E. Mazur, and D. E. Ingber. Visco-
elastic retraction of single living stress fibers and its impact on
cell shape, cytoskeletal organization, and extracellular
matrix mechanics. *Biophys. J.* 90:3762–3773, 2006.
¹⁷Landau, L. D., and E. M. Lifshitz. *Theory of Elasticity.*
New York: Pergamon Press, 1981.
¹⁸Lele, T. P., J. Pendse, S. Kumar, M. Salanga, J. Karavitis,
and D. E. Ingber. Mechanical forces alter zyxin unbinding
kinetics within focal adhesions of living cells. *J. Cell.*
Physiol. 207:187–194, 2006.
¹⁹Lindemann, C. B., and A. J. Hunt. Does axonemal dynein
push, pull, or oscillate? *Cell Motil. Cytoskeleton* 56:237–
244, 2003.
²⁰Llopis, I., M. C. Lagomarsino, I. Pagonabarraga, and C. P.
Lowe. Cooperativity and hydrodynamic interactions in
externally driven semiflexible filaments. *Comput. Phys.*
Commun. 179:150–154, 2008.
²¹Llopis, I., I. Pagonabarraga, M. C. Lagomarsino, and C. P.
C. Lowe. Sedimentation of pairs of hydrodynamically
interacting semiflexible filaments. *Phys. Rev. E* 76:061901,
2007.
²²Lodish, H. F., A. Berk, C. A. Kaiser, M. Krieger, M. P.
Scott, A. Bretscher, H. Ploegh, and P. Matsudaira.
Molecular Cell Biology. New York: W.H. Freeman, 2008.
²³Navone, F., J. Niclas, N. Homboher, L. Sparks, H. D.
Bernstein, G. McCaffrey, and R. D. Vale. Cloning and
expression of a human kinesin heavy chain gene: interac-
tion of the COOH-terminal domain with cytoplasmic
microtubules in transfected CV-1 cells. *J. Cell Biol.*
117:1263–1275, 1992.
²⁴Nedelec, F., and D. C. Foethke. Collective Langevin
dynamics of flexible cytoskeletal fibers. *New J. Phys.* 9:427,
2007.
²⁵O'Connell, C. B., and Y. L. Wang. Mammalian spindle
orientation and position respond to changes in cell shape in
a dynein-dependent fashion. *Mol. Biol. Cell* 11:1765–1774,
2000.
²⁶Reinsch, S., and P. Gonczy. Mechanisms of nuclear posi-
tioning. *J. Cell Sci.* 111:2283–2295, 1998.
²⁷Shelden, E., and P. Wadsworth. Observation and quanti-
fication of individual microtubule behavior in vivo:
microtubule dynamics are cell-type specific. *J. Cell Biol.*
120:935–945, 1993.
²⁸Siegrist, S. E., and C. Q. Doe. Microtubule-induced cortical
cell polarity. *Genes Dev.* 21:483–496, 2007.

- 668 ²⁹Toba, S., T. M. Watanabe, L. Yamaguchi-Okimoto, Y. Y. 675
 669 Toyoshima, and H. Higuchi. Overlapping hand-over-hand 676
 670 mechanism of single molecular motility of cytoplasmic 677
 671 dynein. *Proc. Natl. Acad. Sci. U.S.A.* 103:5741–5745, 2006. 678
 672 ³⁰Umemoto, S., and J. R. Sellers. Characterization of in vitro 679
 673 motility assays using smooth muscle and cytoplasmic 680
 674 myosins. *J. Biol. Chem.* 265:14864–14869, 1990. 681
 682
- ³¹Wu, J., K. C. Lee, R. B. Dickinson, and T. P. Lele. How 675
 dynein and microtubules rotate the nucleus. *J. Cell. Physiol.* 226:2666–2674, 2010. 676
 677
³²Wu, J., G. Misra, R. J. Russell, A. J. C. Ladd, T. P. Lele, 678
 and R. B. Dickinson. Effects of dynein on microtubule 679
 mechanics and centrosome positioning. *Mol. Biol. Cell* 680
 22:4834–4841, 2011. 681
 682

UNCORRECTED PROOF